

# GTestimate: Improving relative gene expression estimation in scRNA-seq using the Good-Turing estimator

Martin Fahrenberger <sup>\*1,2</sup>, Christopher Esk<sup>3,4</sup>, and Arndt von Haeseler<sup>1,5</sup>

<sup>1</sup>Center for Integrative Bioinformatics Vienna (CIBIV), Max Perutz Labs, University of Vienna and Medical University of Vienna, Vienna BioCenter (VBC), Vienna, Austria.

<sup>2</sup>Vienna Biocenter PhD Program, a Doctoral School of the University of Vienna and the Medical University of Vienna, 1030 Vienna, Austria.

<sup>3</sup>Institute of Molecular Biology, University of Innsbruck, Innsbruck, Austria

<sup>4</sup>Institute of Molecular Biotechnology of the Austrian Academy of Science (IMBA), Vienna BioCenter (VBC), Vienna, Austria

<sup>5</sup>University of Vienna, Faculty of Computer Science Bioinformatics and Computational Biology, Vienna, Austria.

August 30, 2024

## <sup>1</sup> Abstract

<sup>2</sup> **Background:** Single-cell RNA-seq suffers from unwanted technical variation between cells, caused by its <sup>3</sup> complex experiments and shallow sequencing depths. Many conventional normalization methods try to <sup>4</sup> remove this variation by calculating the relative gene expression per cell. However, their choice of the <sup>5</sup> Maximum Likelihood estimator is not ideal for this application.

<sup>6</sup> **Results:** We present *GTestimate*, a new normalization method based on the Good-Turing estimator, <sup>7</sup> which improves upon conventional normalization methods by accounting for unobserved genes. To validate <sup>8</sup> *GTestimate* we developed a novel cell targeted PCR-amplification approach (cta-seq), which enables <sup>9</sup> ultra-deep sequencing of single cells. Based on this data we show that the Good-Turing estimator improves <sup>10</sup> relative gene expression estimation and cell-cell distance estimation. Finally, we use *GTestimate*'s compatibility <sup>11</sup> with Seurat workflows to explore three common example data-sets and show how it can improve <sup>12</sup> downstream results.

<sup>13</sup> **Conclusion:** By choosing a more suitable estimator for the relative gene expression per cell, we were able to <sup>14</sup> improve scRNA-seq normalization, with potentially large implications for downstream results. *GTestimate* <sup>15</sup> is available as an easy-to-use R-package and compatible with a variety of workflows, which should enable <sup>16</sup> widespread adoption.

---

<sup>\*</sup>martin.fahrenberger@gmail.com

17 **Keywords**

18 scRNA-seq, Normalization, Gene Expression, Good-Turing estimator, Deep Sequencing, Tar-  
19 geted Amplification

20 **Introduction**

21 Single-cell RNA-seq (scRNA-seq) provides new insights into cell diversity, differentiation and disease [1, 2, 3].  
22 These insights are enabled by affordable high-throughput methods for the parallel sequencing of thousands of  
23 cells [4, 5]. However, they require many experimental steps, whose efficiency differs between cells, leading to  
24 high variability in the number of mRNAs captured. Additionally, sequencing depths as low as 20,000 reads  
25 per cell [6] and the nature of parallel sequencing introduce stochastic variation [5, 7, 8]. After accounting  
26 for PCR-duplicates among reads, a median of  $\sim$ 5,000 UMIs/cell (number of sequenced mRNA molecules  
27 per cell) with a range of  $\sim$ 500-20,000 UMIs/cell is typical for a high quality sample (Fig. 1a). This high  
28 technical variation between cells results in a low signal-to-noise ratio, which makes data analysis challenging.

29 During data processing (Fig. 1b) *global-scaling normalization* methods [8] such as e.g. Seurat's *Normal-*  
30 *izeData* [9], scran's *computeSumFactors* [10, 11] or scanpy's *normalize\_total* [12] account for the variation in  
31 UMIs/cell by calculating a single scaling-factor (or size-factor) per cell. Despite its simplicity, this approach  
32 has been shown to outperform more complex methods [13].

33 *Global-scaling normalization* inherently requires the calculation of the relative gene expression levels per  
34 cell. Although not typically discussed as such, the calculation used by these methods is a Maximum Likeli-  
35 hood estimation (ML) [14] of the relative gene expression frequency per cell.

$$\hat{f}_g^{ML} = \frac{c_g}{\sum_i c_i} \quad (\text{ML})$$

36 where  $c$  denotes the transcriptomic profile of the cell with a count  $c_g$  for each gene  $g$ .

37 However, at  $\sim$ 5,000 UMIs/cell only  $\sim$ 2.5% of the  $\sim$ 200,000 mRNA transcripts in a typical mammalian cell  
38 [15] are sequenced and many expressed genes remain unobserved, as evident by the low genes/cell observed  
39 in scRNA-seq experiments (Suppl. Figure 1). ML then estimates the relative expression of unobserved genes  
40 as zero. This inherently leads to overestimation of the relative expression for observed genes, since the sum  
41 of all relative frequencies equals one ( $\sum_g \hat{f}_g^{ML} = 1$ ).

42 To reduce this overestimation we propose a Simple Good-Turing estimator [16, 17].

$$\hat{f}_g^{GT} = \begin{cases} \frac{(c_g+1)}{\sum_i c_i} \cdot \frac{N_{c_g+1}}{N_{c_g}}, & \text{for } c_g > 0 \\ 0, & \text{for } c_g = 0 \end{cases} \quad (\text{GT})$$

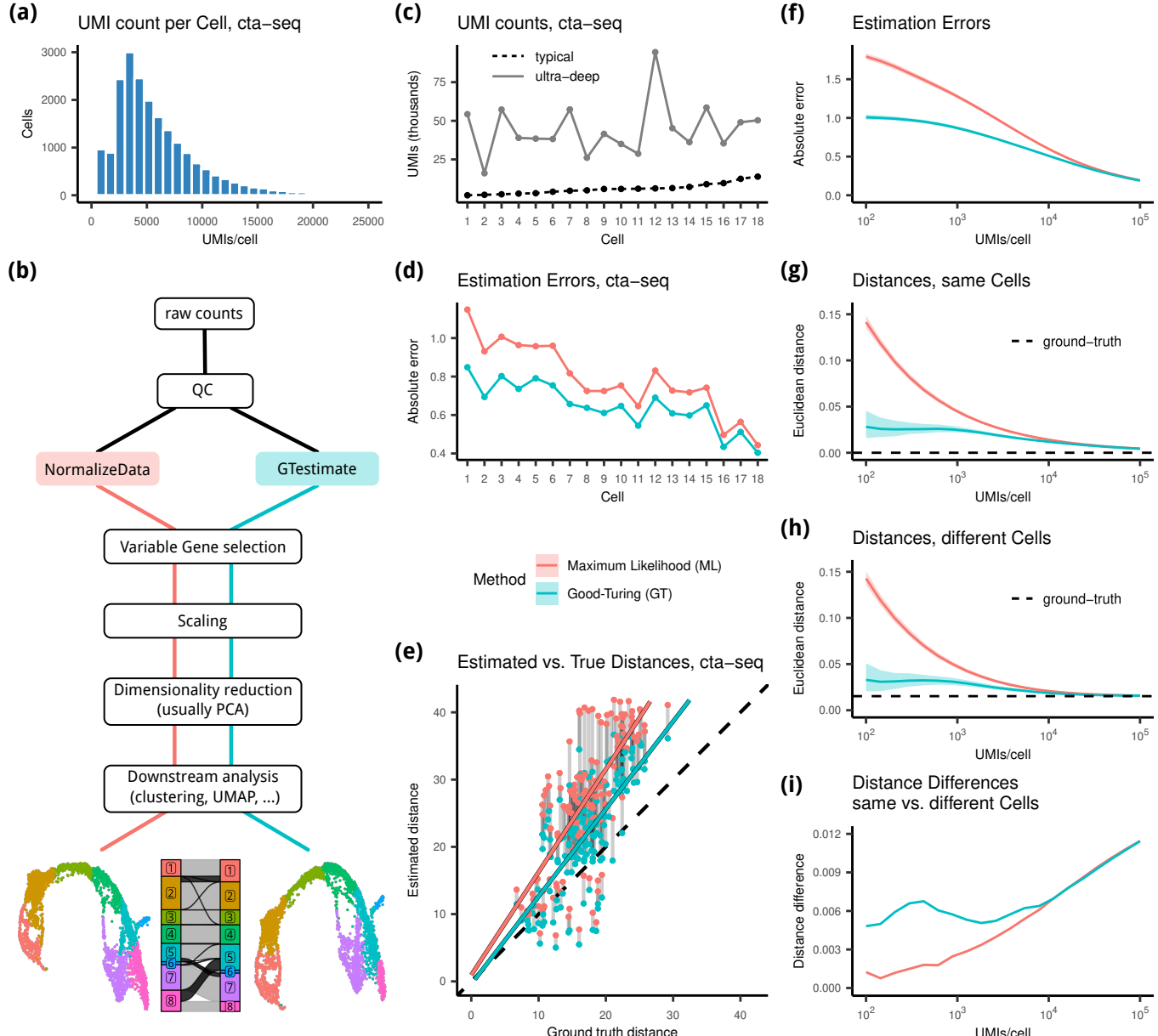


Figure 1: (a) Histogram of  $UMIs/cell$  for 17,653 cells in the cta-seq experiment before amplification. (b) Schema of a scRNA-seq analysis showing where *GTestimate* integrates into the workflow. (c)  $UMIs/cell$  for the 18 selected cells in the cta-seq experiment, before (*typical*) and after (*ultra-deep*) amplification. Cells ordered based on  $UMIs/cell$  in the *typical* cta-seq data. (d) Absolute error of the relative gene expression estimation in the cta-seq experiment. (e) Euclidean cell-cell distances in PCA-space in the cta-seq experiment. (f) Average absolute estimation error of the relative gene expression of a cell when subsampled to different  $UMIs/cell$ . (g-h) Mean Euclidean cell-cell distance in relative gene expression space, between two independent random samples of the same cell (g) between independent random samples of two different cells (h). (i) Difference between the mean cell-cell distances in (g) and (h). Colored ribbons in (f,g,h) represent the 5% – 95% quantile range.

43 where  $N_{c_g}$  denotes the number of genes with count  $c_g$  in the cell.

44 GT adjusts the relative expression estimates of observed genes, particularly those with low counts, based  
45 on the frequency of each count value in the cell. This even enables an estimate for the relative expression of  
46 unobserved genes (for further details see Suppl. Info. 1.1).

47 In this study, we first compare the performance of GT and ML on novel ultra-deep sequencing data,  
48 and then show how GT improves downstream results, by integrating it into standard scRNA-seq analysis  
49 workflows. To achieve this we developed *GTestimate*, a new scRNA-seq normalization method centered  
50 around GT. *GTestimate* is an easy-to-use R-package designed to seamlessly replace Seurat's *NormalizeData*.

## 51 Results

### 52 ultra-deep sequencing of single cells

53 Comparison between GT and ML requires ground-truth transcriptomic profiles of single cells. However,  
54 current simulation software cannot adequately emulate the complexity of scRNA-seq data and the choice  
55 of simulator may affect benchmarking results [18]. We therefore designed a cell targeted PCR-amplification  
56 strategy (cta-seq), which enabled us to sequence a small set of selected cells, from a *typical* sequencing run,  
57 a second time at a *ultra-deep* sequencing depth. This *ultra-deep* sequencing data contains an average of 23  
58 million reads per cell, a stark contrast to the average 16,965 reads for the same cells in the *typical* data  
59 (Suppl. Figure 2). This led to a ~7.4 fold increase in *UMIs/cell* (Fig. 1c) and a ~3.3 fold increase in  
60 *genes/cell* (Suppl. Figure 3). We then used the relative gene expression levels of these *ultra-deep* profiles as  
61 the ground-truth for these cells.

### 62 Performance of GT and ML

63 Based on the cta-seq data we then evaluated GT and ML. When we applied GT and ML to the *typical* profiles  
64 and compared the results to the ground-truth, GT consistently showed a lower estimation error across all 18  
65 cells, by ~17% on average (Fig. 1d).

66 Relative gene expression profiles are the basis of most scRNA-seq analysis (Fig. 1b), such as the calculation  
67 of cell-cell distances in PCA-space (often used as a measure for the similarity between two cells). We therefore  
68 also calculated cell-cell distances between the *typical* profiles, once based on GT and once based on ML, and  
69 compared the results to the cell-cell distances between the *ultra-deep* profiles. We observed a 36% reduction  
70 of the distance estimation error when using GT instead of ML (Fig. 1e, Suppl. Table 1).

71 Since *UMIs/cell* vary drastically (Fig. 1a) we further assessed the performance of GT and ML at different  
72 *UMIs/cell*. We applied GT and ML to random subsamples of the cell with the highest *UMIs/cell* in the  
73 *ultra-deep* cta-seq data (Cell 12, at 94,440 UMIs) and compared the estimates to the ground-truth expression

74 profile of this cell. Similar to before (Fig. 1d) the estimation error for both GT and ML decreased with  
75 increasing *UMIs/cell* and GT consistently showed a lower error than ML, especially at low *UMIs/cell* (Fig.  
76 1f).

77 Next, we assessed the impact of *UMIs/cell* on cell-cell distances. We first compared the mean distance  
78 between two random samples of the same cell (cell 12), both sampled to the same *UMIs/cell*. This distance  
79 was calculated in relative gene expression space and should approach zero for high *UMIs/cell*. However,  
80 ML led to grossly overestimated distances at small *UMIs/cell* (Fig. 1g). The estimated distance after ML  
81 additionally showed strong correlation to the *UMIs/cell*, which is problematic as we assume that most of the  
82 observed variation in *UMIs/cell* is technical noise. In contrast, GT did not show correlation to the *UMIs/cell*  
83 and demonstrated lower distance estimation errors overall.

84 We then examined the distances between two distinct cells by also drawing random samples from the cell  
85 with the second highest *UMIs/cell* in the *ultra-deep* cta-seq data (cell 15, at 58,589 UMIs), which is of a  
86 different cell-type. We calculated the distances between the sampled profiles of cell 12 and cell 15 at varying  
87 *UMIs/cell*. We again saw large overestimation of the distances when using ML, while using GT strongly  
88 reduced this error. For high *UMIs/cell* the estimated distances converged to the true distance of 0.015 (Fig.  
89 1h).

90 When based on ML, the estimated distances between identical cells (Fig. 1g) and distinct cells (Fig. 1h)  
91 were almost the same for low *UMIs/cell*. This makes it very difficult to e.g. distinguish between cell-types.  
92 However, when we used GT as the basis for these distances we saw a much clearer separation between  
93 identical cells and cells of different cell-type, for cells with < 10,000 *UMIs/cell* (Fig. 1i).

#### 94 ***GTestimate*'s impact on downstream results**

95 After showing GT's advantages for relative gene expression estimation and cell-cell distance estimation, we  
96 examined how our GT based normalization method *GTestimate* impacts downstream results. The difference  
97 between *GTestimate* and other *global-scaling normalization* methods is only in the estimator used, all other  
98 settings can be adjusted to be equivalent to e.g. scran's *computeSumFactors* or scanpy's *normalize\_total*. At  
99 default settings *GTestimate* behaves identically to *NormalizeData*, including the same log-transformation.  
100 We therefore used *NormalizeData*, as a representative of ML based *global-scaling normalizations* for all  
101 following comparisons. However, we would expect similar results when comparing to other *global-scaling*  
102 *normalization* methods.

103 We first assessed *GTestimate*'s impact on cell-type clustering by reanalyzing the pbmc3k data-set of  
104 peripheral blood mononuclear cells [19]. Here, normalization with *GTestimate* instead of *NormalizeData*  
105 resulted in 4.6% of cells being assigned to a different cluster (Fig. 2a), mostly among the Naive CD4 T-cells,

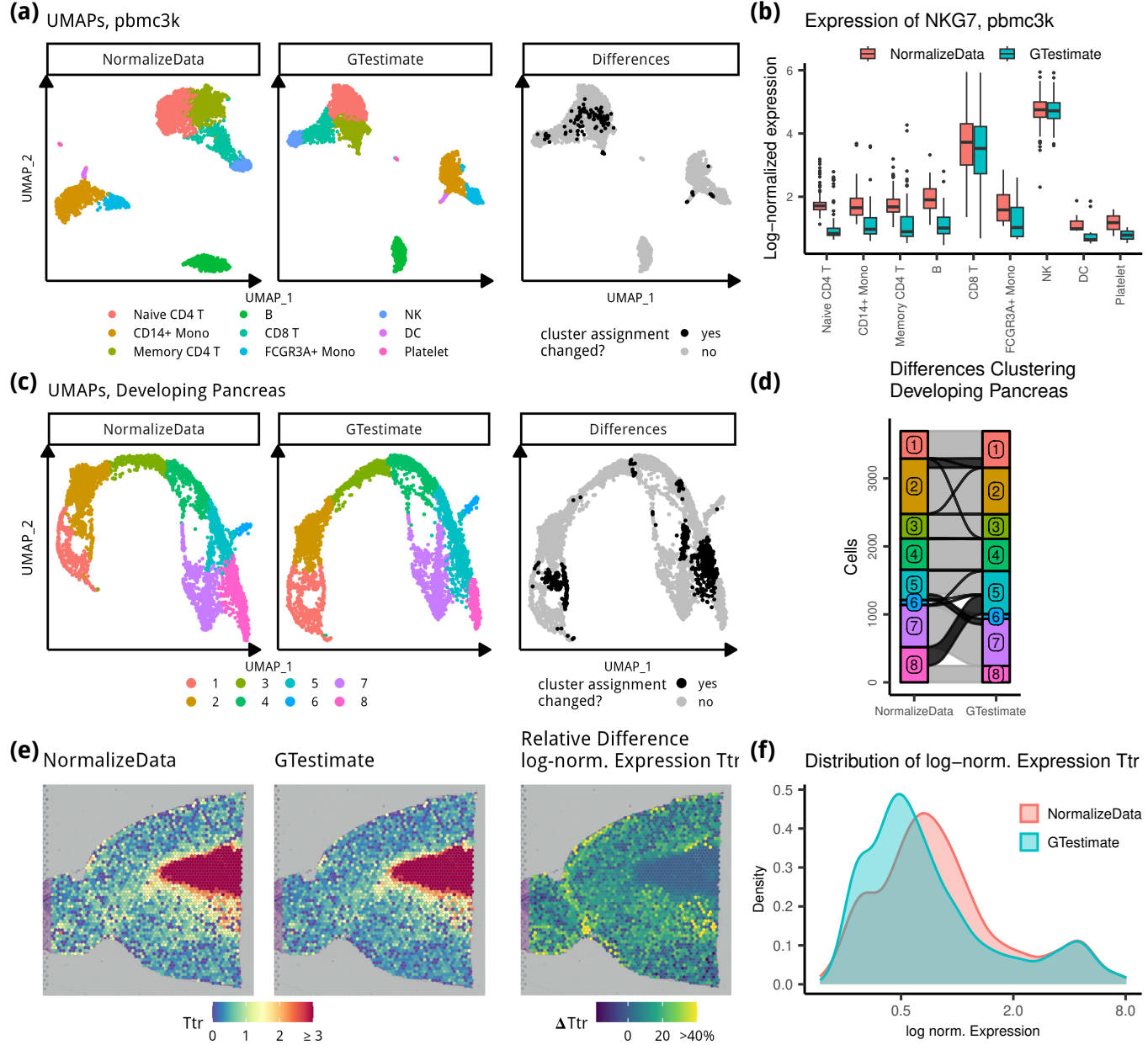


**Figure 2: pbmc3k:** (a) UMAPs based on *NormalizeData* and *GTestimate*, and UMAP highlighting differences in cluster assignment. (b) Boxplot showing log-normalized expression of *NKG7* per cell-type (zeroes not shown). **Developing Pancreas:** (c) UMAPs based on *NormalizeData* and *GTestimate*, and UMAP highlighting differences in cluster assignment. (d) Sankey diagram showing the differences in cluster assignment based on *NormalizeData* and *GTestimate*. **Spatial Transcriptomics:** (e) log-normalized gene expression of *Ttr* based on *NormalizeData* and *GTestimate* as well as percent difference in log-normalized expression of *Ttr* between *NormalizeData* and *GTestimate*. (f) Density plot showing the distribution of log-normalized gene expression values of *Ttr* for *NormalizeData* and *GTestimate*.

106 Memory CD4 T-cells and CD8 T-cells.

107 We additionally analyzed a developing pancreas data-set [20], characterized by more gradual cell-type trans-  
108 sitions compared to the pbmc3k data-set. After normalization with *GTestimate* instead of *NormalizeData*,  
109 14.6% of cells were assigned to a different cluster (Fig. 2c,d).

110 While the correct classification of cells in both of these data-sets remains unknown, our results in Fig. 1  
111 suggest that *GTestimate* provides a better basis for this classification.

112 To examine the impact of *GTestimate* on the expression estimates of individual genes we considered the  
113 log-normalized expression of cell-type specific marker genes in the pbmc3k data-set. As an example we  
114 used *NKG7* a highly specific NK-cell and *CD8+* T-cell marker [21]. When using *GTestimate* instead of  
115 *NormalizeData*, the log-normalized expression of *NKG7* remained constant in NK-cells and *CD8+* T-cells,  
116 but was reduced in all other cell-types (Fig. 2b). *GTestimate* therefore resulted in clearer separation of  
117 NK-cells and *CD8+* T-cells from other cell-types. We observed this for nearly all marker genes described in  
118 Seurat's pbmc3k tutorial (Suppl. [Figure 4](#)). These differences may explain some of the observed changes in  
119 clustering.

120 Finally, we applied *GTestimate* to the spot-wise normalization of a Spatial Transcriptomics data-set of the  
121 mouse brain [22]. In this data-set, normalization with *GTestimate* and *NormalizeData* resulted in 17 and  
122 19 clusters respectively (Suppl. [Figure 5](#), [Figure 6](#), [Figure 7](#)), we therefore refrained from any cluster based  
123 comparisons of *GTestimate* and *NormalizeData*. However, the spatial coordinates enabled examination of  
124 area specific marker genes, independent of the clustering. As an example we considered the log-normalized  
125 expression of the choroid plexus marker gene *Ttr* (Fig. 2e). When using *GTestimate* we saw a reduction of  
126 the unspecific expression of *Ttr* for spots outside the choroid plexus. Here, *GTestimate* showed up to 50%  
127 reduction of the log-normalized expression, compared to *NormalizeData*, while expression estimates inside  
128 the choroid plexus remained constant (Fig. 2e). This resulted in clearer separation of the choroid plexus  
129 spots from the surrounding tissue as shown by the distribution of expression values of *Ttr* (Fig. 2f).

130 When we additionally considered the *UMIs/spot* ([Figure 8](#)), we saw a negative correlation between the  
131 change in log-normalized expression of *Ttr* and *UMIs/spot*. This supports previous observations that  
132 *NormalizeData* overestimates the expression of *Ttr* in areas with low *UMIs/spot*. Whereas, *GTestimate*  
133 reduces this overestimation and improves the signal-to-noise ratio.

## 134 Discussion

135 In summary, the estimation of relative gene expression is a central part of scRNA-seq data analysis, which  
136 has not received the same attention as other steps. We have shown that replacing the standard ML with GT  
137 improves relative gene expression estimation, without requiring expensive computations. By improving the

138 signal-to-noise ratio at this basic level, our new normalization method *GTestimate* can have large impact on  
139 downstream results.

140 In the validation we avoided potential issues with simulated data by employing a novel cell targeted PCR-  
141 amplification strategy to sequence the same cells at two vastly different *UMIs/cell*. This strategy may also  
142 be useful in other areas, such as the study of rare cell-types. Additionally, the resulting data-set may serve  
143 as a benchmark for other methods.

144 *GTestimate* is available as an open-source R-package (<https://www.github.com/Martin-Fahrenberger/GTestimate>) and works with all common scRNA-seq data-formats. While *GTestimate*'s default behavior is  
145 designed to seamlessly replace *NormalizeData* it is also compatible with a wide variety of other workflows.  
146

## 147 Materials and Methods

### 148 Implementation of *GTestimate*

149 The user-facing section of our *GTestimate* package was developed in R and handles input and output in the  
150 various supported data-formats. The core implementation of the Simple Good-Turing estimator is written  
151 in C++ and is heavily based on Aaron Lun's implementation for the edgeR R-package [23]. This core  
152 implementation includes the linear smoothing, which is necessary due to the sparsity of the frequencies of  
153 frequencies vector (i.e the frequency of the count values). It further includes a rescaling step which ensures  
154 that the estimated relative expression frequencies of all observed genes, plus the sum of probabilities of all  
155 unobserved genes (Suppl. Info. 1.1), add up to exactly one [17].

### 156 cta-seq experiment

157 In the cta-seq experiment we aimed to sequence a selected set of cells from a *typical* scRNA-seq library again  
158 at a *ultra-deep* sequencing depth. However, due to sequencing-saturation this quickly becomes prohibitively  
159 expensive. We therefore designed a PCR based cell targeted amplification strategy (cta-seq), to selectively  
160 amplify all transcripts from a small set of cells, through the use of primers specific to their cell-barcode. This  
161 is similar to the TAP-seq protocol [24], which uses gene-specific primers to amplify all transcripts of certain  
162 genes.

### 163 Sequencing cta-seq, *typical*

164 To ensure high quality input material we used leftover cDNA from a previously sequenced sample [25], which  
165 had shown high *UMIs/cell* and *genes/cell*. The sample was taken out of -20°C storage and prepared for  
166 Illumina sequencing at the Vienna Biocenter Next Generation Sequencing facility using 10X Dual Index Kit  
167 TT. We then split the resulting sequencing library into two aliquots and stored the second halve again at

168 -20°C. The first halve was sequenced on a Illumina NovaSeq S4 in paired-end mode with 2x150bp read length  
169 and 400 million reads.

170 **Sequencing cta-seq, *ultra-deep***

171 Based on the results from the *typical* sequencing run we selected 18 cells of interest for the cta-seq experiment  
172 (see below). For these 18 cells we designed PCR primers specific to their cell-barcodes. We then used the  
173 second aliquote of the previously prepared sequencing library to perform three rounds of PCR amplification on  
174 it using AmpliTaq Gold 360 MM (ThermoFisher, cat.: 4398886) supplemented with EvaGreen dye (Biotium,  
175 cat.: 31000). We used the following programs in a total volume of 50 $\mu$ l.. PCR1: 1. 95C, 10min; 2. 62C,  
176 30s; 3. 72C, 2min.; 4. Return to 2. x2; 5. 95C, 25s; 6. 62C, 30s; 7. 72C, 2min, fluorescence measurement;  
177 8. 72C, 15s; 9. return to 5. x16. PCR2: 1. 95C, 10min; 2. 62C, 30s; 3. 72C, 2min.; 4. Return to 2. x2;  
178 5. 95C, 25s; 6. 62C, 30s; 7. 72C, 2min, fluorescence measurement; 8. 72C, 15s; 9. return to 5. x16. PCR3:  
179 1. 95C, 10min; 2. 67C, 30s; 3. 72C, 2min.; 4. Return to 2. x2; 5. 95C, 25s; 6. 67C, 30s; 7. 72C, 2min,  
180 fluorescence measurement; 8. 72C, 15s; 9. return to 5. x8. Reactions were stopped in step 8 according to  
181 fluorescent measurements in log phase. Reaction input in PCRs 2 and 3 were 0.5  $\mu$ l of the previous reaction.  
182 Resulting reactions were purified, and pooled for Illumina sequencing on a NovaSeq S4 in paired-end mode  
183 with 2x150bp read length and 400 million reads. The primer sequences used can be found in Suppl. Table  
184 1, PCR1 primers were designed with varying length to achieve similar melting temperatures.

185 **Data Analysis**

186 All data analysis was performed in R (v4.3.1) using Seurat (v5.0.0) functions at default settings unless stated  
187 otherwise.

188 **Data analysis, cta-seq *typical* depth**

189 We first processed the *typical* depth sequencing data using CellRanger (v7.1.0), this resulted in 20,214  
190 cells. During cell QC we then removed all cells expressing  $\leq$  1000 or  $\geq$  5000 genes as well as cells with  
191  $\geq 8\%$  mitochondrial reads, with 17,653 cells remaining. We then normalized with Seurat's *NormalizeData*,  
192 selected the top 2000 most variable genes and performed gene-wise z-score scaling. Next we applied PCA  
193 and performed unsupervised clustering of cells using the Louvain algorithm [26](resolution = 0.1), based on  
194 the first 50 principal components (PCs). This resulted in four cell-type clusters, the smallest cluster (with  
195 only 504 cells) was excluded from the subsequent analysis.

196 From the remaining 17,149 cells we selected 18 cells for targeted amplification, six cells from each of the  
197 three remaining clusters. To select a diverse set of cells from each cluster we used the following:

198 1. We identified the two nearest neighbors for each cell (in PCA space).

199 2. We excluded cells for which at least one nearest neighbor belonged to a different cluster.

200 3. For the remaining 16,295 cells, we computed the #UMI-rank, from the number of observed UMIs per

201 cell (ties were broken randomly).

202 4. Similarly, we computed the  $\frac{\#UMI}{\#Genes}$ -rank based on the ratio of the number of observed UMIs and the

203 number of observed genes in the cell (ties were broken randomly).

204 5. Subsequently, we calculated the diversity of each cell and its neighbors as the area of the induced

205 triangle of the cell and its neighbors in a #UMI-rank x  $\frac{\#UMI}{\#Genes}$ -rank plot. The six cells from the two

206 most diverse neighborhoods (i.e. largest triangle area) were selected for amplification.

207 These steps were designed to cover a diverse set of cells for which the various experimental steps had varying

208 efficiencies. The selection of triplets from the same neighborhoods provided groups of cells with similar gene

209 expression patterns, while the number of UMIs and the number of observed genes were used as proxies for

210 the mRNA capture efficiencies and the health of the isolated cells.

## 211 Data analysis, cta-seq *ultra-deep*

212 The sequencing data from the *ultra-deep* sequencing run were processed using CellRanger (v7.1.0).

213 However, due to the high number of PCR cycles during amplification, and the resulting high number

214 of reads for the 18 selected cells, CellRanger's UMI correction approach was no longer sufficient. Manual

215 inspection of the reads showed that errors in the UMI sequences had inflated the number of unique reads.

216 This was further exacerbated by a faulty implementation of the UMI-correction approach in the CellRanger

217 software by 10X Genomics. CellRanger erroneously corrects UMIs containing sequencing errors towards other

218 UMIs that also contain sequencing errors. E.g. If we have 3 UMIs: AAAA with 10 reads, AAAT with 2

219 reads and AATT with 1 read, AATT would be corrected towards AAAT (Hamming Distance 1) and stay

220 as AAAT, even though the original 2 AAAT reads would be corrected to AAAA in the same step. We have

221 reported this issue to 10X Genomics on 13th of July 2023, 10X Genomics acknowledge the issue on 14th of

222 July 2023. The issue remains unresolved in CellRanger 7.2.0 (released on the 10th of November, 2023).

223 To circumvent these issues we extracted the relevant information for each read (count, ensemble gene id,

224 cell-barcode, uncorrected UMI and CellRanger corrected UMI) from the possorted\_genome\_bam.bam as

225 provided by CellRanger and replicated CellRanger's read counting workflow in R. As a sanity-check we first

226 used the CellRanger corrected UMIs and achieved the exact same count-matrix as CellRanger. We then

227 used the raw UMIs instead of the CellRanger corrected UMIs, implemented the UMI-tools directional UMI

228 correction approach [27] in R and applied it to correct the UMIs for the 18 selected cells, we then counted

229 again. The resulting count-matrix showed differences for 28% of the non-zero entries when compared to the  
230 CellRanger results. We used these improved counts for the *ultra-deep* profiles in all further analysis.

231 **Comparison of GT and ML using cta-seq**

232 To evaluate the performance of GT and ML based on the cta-seq data-set we estimated the relative gene  
233 expression for the 18 selected cells by applying both estimators to the *typical* transcriptomic profiles.

234 The relative gene expression for the ground-truth *ultra-deep* profiles was estimated with ML. We chose ML  
235 to be conservative regarding the performance of GT and since the overestimation due to unobserved genes  
236 should be small for the *ultra-deep* profiles Suppl. [Figure 9](#).

237 **Relative gene expression estimation**

238 We calculated the absolute estimation error for the relative gene expression of the 18 cells by comparing the  
239 estimation results of GT and ML based on the *typical* transcriptomic profiles to the ground-truth relative  
240 gene expression of the *ultra-deep* profiles. We consider the relative gene expression estimation error of a cell  
241 to be the sum of the individual relative gene expression estimation errors in the cell.

242 **Cell-cell distances**

243 The pairwise Euclidean distances between the 18 cells were calculated in PCA space (as is common for  
244 cell-cell distances in scRNA-seq). However, to keep the necessary projections similar to a regular scRNA-seq  
245 analysis this space could not simply be constructed based only on the 18 selected cells.

246 Instead we calculated the projections based on 17,653 cells in the *typical* sequencing run. After normal-  
247 ization there are three pre-processing steps which all depend on the context of a full data-set; Variable gene  
248 selection, gene-wise z-score scaling and PCA.

249 To keep these steps identical for both the GT and ML profiles of the *typical* sequenced cells, as well as the  
250 *ultra-deep* profiles we performed them using customized functions. We used the same list of variable genes  
251 (calculated based on all 17,653 cells) for the analysis of all profiles. We then scaled the genes in all profiles  
252 using the mean and standard deviation of genes calculate based on the full 17,653 cells. Finally we projected  
253 all profiles into the same 50 dimensional PCA-space calculated from the full 17,653 cells.

254 In this PCA-space we calculated the pairwise distances between the ML profiles, between the GT profiles  
255 as well as between the ground-truth *ultra-deep* profiles. We then compared the resulting non-zero distances  
256 based on GT and ML to the ground-truth *ultra-deep* distances.

## 257 Comparison of GT and ML at different *UMIs/cell*

258 When analyzing the impact of *UMIs/cell* on the estimation performance we used the cell with the highest  
259 number of UMIs after amplification (cell 12, cell-barcode TCTCTGGGTGTGCTTA) and the cell with the  
260 second highest number of UMIs after amplification (cell 15, cell-barcode GGCTTTCGTGTGTCGC).

261 We generated 1000 randomly sampled profiles at each *UMIs/cell* level by drawing genes from the *ultra-deep*  
262 count-vector, weighted by count and with replacement. The 20 *UMIs/cell* levels at which we sampled were  
263 chosen equidistant in log10-space from 100 to 100,000 (i.e. 100, 143, 206, 297, 428, 615, 885, 1274, 1832,  
264 2636, 3792, 5455, 7847, 11288, 16237, 23357, 33598, 48329, 69519, 100000 *UMIs/cell*). We then applied GT  
265 and ML respectively to these sampled profiles to estimate their relative gene expression.

## 266 Relative gene expression estimation

267 To asses the relative gene expression estimation performance of GT and ML we compared their estimates  
268 for each sampled profile from cell 12 to the relative gene expression of the full *ultra-deep* profile of cell 12,  
269 and calculated the absolute error.

## 270 Cell-cell distance estimation

271 To asses cell-cell distance estimation performance we calculated the Euclidean distances between the relative  
272 gene expression profiles of pairs of sampled profiles (either from cell 12 twice or from cell 12 and cell 15)  
273 based on GT and ML. We calculated the true distance based on the full *ultra-deep* profiles.

## 274 Downstream analysis

### 275 Data analysis, pbmc3k

276 The pbmc3k data-set was downloaded from 10X Genomics [19] and processed following Seurat's "Guided  
277 Clustering Tutorial" [28]. In short:

278 During QC we filtered out genes expressed in less than 3 cells, and cells with less than 200 expressed genes.  
279 We then filtered out cells with > 5% mitochondrial reads and finally we removed all cells expressing more  
280 than 2,500 genes.

281 During preprocessing cells were normalized using either Seurat's *NormalizeData* or *GTestimate* at default  
282 settings. For both normalization methods individually, we then identified variable genes and z-score scaled the  
283 data, followed by calculation of the top 10 PCs. Based on these PCs we then constructed the neighborhood  
284 graphs and performed unsupervised Louvain clustering (resolution = 0.5). Finally we calculated the UMAP  
285 for both conditions and annotated clusters based on marker gene expression, following the Seurat tutorial.

286 **Data analysis, developing pancreas**

287 The pancreas endocrinogenesis day15 dataset was downloaded [29] and imported into R to be processed  
288 using Seurat. We only used the spliced counts and normalized them using *GTestimate* and *NormalizeData*;  
289 from there on all following steps were performed identically for the two approaches.

290 First we identified variable genes and performed gene-wise z-score scaling, followed by calculation of the  
291 top 50 PCs. Based on the PCs we constructed the neighborhood graph and performed unsupervised Louvain  
292 clustering (resolution = 0.4). Finally we calculated the UMAP.

293 We manually adjusted the cluster numbering (and thereby their color) for Fig. 2c and Fig. 2d. to have  
294 consistent cluster-colors from left to right.

295 **Data analysis, Spatial Transcriptomics**

296 The stxBrain data-set of sagital mouse brain slices from 10X Genomics was downloaded using the SeuratData  
297 R-package. In our analysis we focused on the anterior1 slice of the data-set following Seurat's "Analysis of  
298 spatial datasets (Sequencing-based)" vignette [30].

299 Our analysis differs from the vignette only in the normalization methods used. While the vignette uses  
300 *sctransform*[31] for spot-wise normalization we instead used *NormalizeData* and *GTestimate*. Direct compar-  
301 ison of GT and ML to *sctransform* on the basis of relative gene expression is not possible, since *sctransform*  
302 does not calculate relative gene expression levels. Normalization was followed by variable gene selection and  
303 gene-wise scaling. We then calculated the first 30 PCs and used them to construct the neighborhood graph,  
304 perform unsupervised Louvain clustering and calculate the UMAP.

305 **Availability of supporting source code and requirements**

- 306 1. Project name: *GTestimate*  
307 2. Project home page: <https://github.com/Martin-Fahrenberger/GTestimate>  
308 3. Operating system(s): Platform independent  
309 4. Programming language: R, C++  
310 5. Other Requirements: devtools, sparseMatrixStats  
311 6. License: GPL3

312 *GTestimate* is available as an open-source R-package on github (<https://www.github.com/Martin-Fahrenberger/GTestimate>). All code for the analysis in this paper, from raw-data to figures, is available on github  
313 (<https://www.github.com/Martin-Fahrenberger/GTestimate-Paper>).

## 315 Data Availability

316 Processed cta-seq data, such as count-matrices, are available via GEO (<https://www.ncbi.nlm.nih.gov/geo/>), accession number GSE268930. Due to patient privacy concerns raw sequencing data will be made  
317 available through controlled access at the European Genome-Phenome Archive (EGA) upon publication.  
318

## 319 List of Abbreviations

320 cta-seq: cell targeted PCR-amplification followed by sequencing; GT: Good-Turing estimator; ML: Maximum  
321 Likelihood estimator; PC: principal component; scRNA-seq: single-cell RNA-sequencing;

## 322 Competing interests

323 The authors declare that they have no competing interests.

## 324 Funding

325 This work was supported by the network grant of the European Commission H2020-MSCA-ITN-2017-765104  
326 “MATURE-NK” to AvH; MF was a fellow in the project. MF was further supported by the Austrian Science  
327 Fund (FWF) project number F78 to AvH.

## 328 Authors' contributions

329 MF and AvH conceived this project, CE and MF developed cta-seq, CE performed the cta-seq wet-lab  
330 experiments, MF implemented GTestimate and analyzed the data. MF wrote the manuscript with input  
331 from CE and AvH. All authors read and approved the final version of the manuscript.

## 332 Acknowledgments

333 We thank Oliver L. Eichmüller for contributing the cDNA-library used in the cta-seq experiment and for his  
334 feedback during discussions. We thank all members of CIBIV for their valuable feedback throughout this  
335 project. We also thank Thomas Grentzinger from the Vienna BioCenter Core Facilities GmbH (VBCF) Next  
336 Generation Sequencing Unit for consultation and sequencing.

## 337 References

338 [1] Aviv Regev, Sarah A Teichmann, Eric S Lander, Ido Amit, Christophe Benoist, Ewan Birney, Bernd  
339 Bodenmiller, Peter Campbell, Piero Carninci, Menna Clatworthy, et al. The human cell atlas. *elife*, 6:  
340 e27041, 2017.

- 341 [2] Jeffrey A Farrell, Yiqun Wang, Samantha J Riesenfeld, Karthik Shekhar, Aviv Regev, and Alexander F  
342 Schier. Single-cell reconstruction of developmental trajectories during zebrafish embryogenesis. *Science*,  
343 360(6392):eaar3131, 2018.
- 344 [3] Jihwan Park, Rojesh Shrestha, Chengxiang Qiu, Ayano Kondo, Shizheng Huang, Max Werth, Mingyao  
345 Li, Jonathan Barasch, and Katalin Suszták. Single-cell transcriptomics of the mouse kidney reveals  
346 potential cellular targets of kidney disease. *Science*, 360(6390):758–763, 2018.
- 347 [4] Evan Z Macosko, Anindita Basu, Rahul Satija, James Nemesh, Karthik Shekhar, Melissa Goldman, Itay  
348 Tirosh, Allison R Bialas, Nolan Kamitaki, Emily M Martersteck, et al. Highly parallel genome-wide  
349 expression profiling of individual cells using nanoliter droplets. *Cell*, 161(5):1202–1214, 2015.
- 350 [5] Grace XY Zheng, Jessica M Terry, Phillip Belgrader, Paul Ryvkin, Zachary W Bent, Ryan Wilson,  
351 Solongo B Ziraldo, Tobias D Wheeler, Geoff P McDermott, Junjie Zhu, et al. Massively parallel digital  
352 transcriptional profiling of single cells. *Nature communications*, 8(1):14049, 2017.
- 353 [6] 10X Genomics. Technical Note - Chromium Single Cell 3' v3: Reagent, Workflow & Software Updates,  
354 25 Febuary, 2019. Document Number CG000201, Rev A.
- 355 [7] Allon M Klein, Linas Mazutis, Ilke Akartuna, Naren Tallapragada, Adrian Veres, Victor Li, Leonid  
356 Peshkin, David A Weitz, and Marc W Kirschner. Droplet barcoding for single-cell transcriptomics  
357 applied to embryonic stem cells. *Cell*, 161(5):1187–1201, 2015.
- 358 [8] Catalina A Vallejos, Davide Risso, Antonio Scialdone, Sandrine Dudoit, and John C Marioni. Nor-  
359 malizing single-cell rna sequencing data: challenges and opportunities. *Nature methods*, 14(6):565–571,  
360 2017.
- 361 [9] Andrew Butler, Paul Hoffman, Peter Smibert, Efthymia Papalexi, and Rahul Satija. Integrating single-  
362 cell transcriptomic data across different conditions, technologies, and species. *Nature biotechnology*, 36  
363 (5):411–420, 2018.
- 364 [10] Aaron TL Lun, Davis J McCarthy, and John C Marioni. A step-by-step workflow for low-level analysis  
365 of single-cell rna-seq data with bioconductor. *F1000Research*, 5, 2016.
- 366 [11] Aaron T L Lun, Karsten Bach, and John C Marioni. Pooling across cells to normalize single-cell rna  
367 sequencing data with many zero counts. *Genome biology*, 17(1):1–14, 2016.
- 368 [12] F Alexander Wolf, Philipp Angerer, and Fabian J Theis. Scanpy: large-scale single-cell gene expression  
369 data analysis. *Genome biology*, 19:1–5, 2018.

- 370 [13] Constantin Ahlmann-Eltze and Wolfgang Huber. Comparison of transformations for single-cell rna-seq  
371 data. *Nature Methods*, pages 1–8, 2023.
- 372 [14] Ronald A Fisher. On the mathematical foundations of theoretical statistics. *Philosophical transactions  
373 of the Royal Society of London. Series A, containing papers of a mathematical or physical character*,  
374 222(594-604):309–368, 1922.
- 375 [15] Ehud Shapiro, Tamir Biezuner, and Sten Linnarsson. Single-cell sequencing-based technologies will  
376 revolutionize whole-organism science. *Nature Reviews Genetics*, 14(9):618–630, 2013.
- 377 [16] Irving J Good. The population frequencies of species and the estimation of population parameters.  
378 *Biometrika*, 40(3-4):237–264, 1953.
- 379 [17] William A Gale and Geoffrey Sampson. Good-turing frequency estimation without tears. *Journal of  
380 quantitative linguistics*, 2(3):217–237, 1995.
- 381 [18] Helena L Crowell, Sarah X Morillo Leonardo, Charlotte Soneson, and Mark D Robinson. The shaky  
382 foundations of simulating single-cell rna sequencing data. *Genome Biology*, 24(1):1–19, 2023.
- 383 [19] 10X Genomics. 3k PBMCs from a Healthy Donor, Single Cell Gene Expression Dataset by Cell Ranger  
384 1.1.0, 26 May, 2016.
- 385 [20] Aimée Bastidas-Ponce, Sophie Tritschler, Leander Dony, Katharina Scheibner, Marta Tarquis-Medina,  
386 Ciro Salinno, Silvia Schirge, Ingo Burtscher, Anika Böttcher, Fabian J Theis, et al. Comprehensive  
387 single cell mrna profiling reveals a detailed roadmap for pancreatic endocrinogenesis. *Development*, 146  
388 (12):dev173849, 2019.
- 389 [21] Martin A Turman, Toshio Yabe, Cynthia McSherry, Fritz H Bach, and Jeffrey P Houchins. Character-  
390 ization of a novel gene (nkg7) on human chromosome 19 that is expressed in natural killer cells and t  
391 cells. *Human immunology*, 36(1):34–40, 1993.
- 392 [22] 10X Genomics. Mouse Brain Serial Section 1 (Sagittal-Anterior), Spatial Gene Expression Dataset by  
393 Space Ranger 1.0.0, 02 December, 2019.
- 394 [23] Yunshun Chen, Lihong Chen, Aaron TL Lun, Pedro L Baldoni, and Gordon K Smyth. edger 4.0:  
395 powerful differential analysis of sequencing data with expanded functionality and improved support for  
396 small counts and larger datasets. *bioRxiv*, pages 2024–01, 2024.
- 397 [24] Daniel Schraivogel, Andreas R Gschwind, Jennifer H Milbank, Daniel R Leonce, Petra Jakob, Lukas  
398 Mathur, Jan O Korbel, Christoph A Merten, Lars Velten, and Lars M Steinmetz. Targeted perturb-seq  
399 enables genome-scale genetic screens in single cells. *Nature methods*, 17(6):629–635, 2020.

- 400 [25] Oliver L Eichmüller, Nina S Corsini, Ábel Vértesy, Ilaria Morassut, Theresa Scholl, Victoria-Elisabeth  
401 Gruber, Angela M Peer, Julia Chu, Maria Novatchkova, Johannes A Hainfellner, et al. Amplification  
402 of human interneuron progenitors promotes brain tumors and neurological defects. *Science*, 375(6579):  
403 eabf5546, 2022.
- 404 [26] Vincent D Blondel, Jean-Loup Guillaume, Renaud Lambiotte, and Etienne Lefebvre. Fast unfolding  
405 of communities in large networks. *Journal of statistical mechanics: theory and experiment*, 2008(10):  
406 P10008, 2008.
- 407 [27] Tom Smith, Andreas Heger, and Ian Sudbery. Umi-tools: modeling sequencing errors in unique molecular  
408 identifiers to improve quantification accuracy. *Genome research*, 27(3):491–499, 2017.
- 409 [28] Satija-Lab. Seurat - guided clustering tutorial, 2023. URL [https://satijalab.org/seurat/articles/pbmc3k\\_tutorial](https://satijalab.org/seurat/articles/pbmc3k_tutorial). Accessed on 13.12.2023.
- 410 [29] Theis Lab. scvelo - github page, 2021. URL [https://github.com/theislab/scvelo\\_notebooks/raw/master/data/Pancreas/endocrinogenesis\\_day15.h5ad](https://github.com/theislab/scvelo_notebooks/raw/master/data/Pancreas/endocrinogenesis_day15.h5ad). Accessed on 13.12.2023.
- 411 [30] Satija-Lab. Analysis, visualization, and integration of spatial datasets with seurat, 2023. URL [https://satijalab.org/seurat/articles/spatial\\_vignette](https://satijalab.org/seurat/articles/spatial_vignette). Accessed on 13.12.2023.
- 412 [31] Saket Choudhary and Rahul Satija. Comparison and evaluation of statistical error models for scrna-seq.  
413 *Genome biology*, 23(1):27, 2022.

## 417 1 Supplementary Materials

### 418 1.1 The Missing Mass

419 Besides improving the relative expression estimates of observed genes, GT can also estimate the sum of the  
420 relative frequencies of all unobserved genes. This can be viewed as the probability  $p_0$  that a next hypothetical  
421 UMI would be of a currently unobserved gene. We have therefore termed  $p_0$  the missing-mass of the relative  
422 gene expression distribution.

423 The missing-mass for each cell is estimated from the number of genes with a UMI count of one ( $N_1$ ) and  
424 the sum of all counts ( $\sum_g c_g$ ) as has previously been discussed [16, 17].

$$\hat{p}_0 = \frac{N_1}{\sum_g c_g} \quad (1)$$

425 When applied to a Seurat or SingleCellExperiment object in R *GTestimate* saves the estimated  $\hat{p}_0$  for each  
426 cell into a meta-data vector called "missing\_mass".

427 The Simple Good-Turing estimator scales the relative frequencies (including  $p_0$ ) to ensure

$$\sum_g \hat{f}_g^{GT} + \hat{p}_0 = 1 \quad (2)$$

428 for each cell.

429 Suppl. [Equation 1](#) provides insight into the amount of information present for each cell, which may warrant  
430 further study. E.g. the missing-mass in the cta-seq experiment is substantially reduced after cell targeted  
431 amplification of reads (Suppl. Fig. 9).

432 Due to the typically low  $UMIs/cell$ , this missing mass of a cell in scRNA-seq can be quite substantial  
433 (Suppl. Fig. 10).

434 **1.2 Supplementary Tables**

Method	Slope	Sum of absolute Residuals	Intercept	Sum of absolute Errors
ML	1.529	1511.317	0.955	3258.049
GT	1.302	1263.276	-0.408	2093.645

Table 1: Characteristics of the regression line of the estimated vs. ground-truth distances for the cta-seq data (Fig. 1d).

435 **1.3 Supplementary Figures**

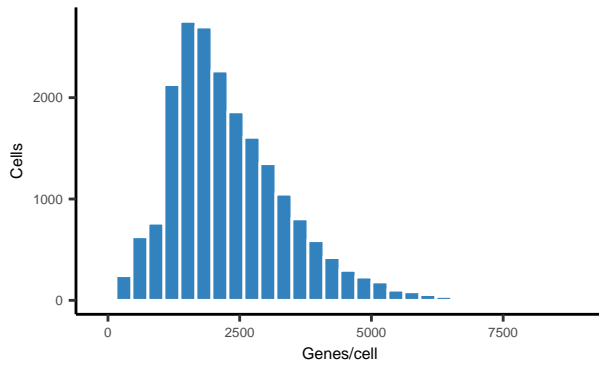


Figure 1: Histogram showing the number of observed genes per cell for the 17,653 cells in the cta-seq sample before amplification (*typical*).

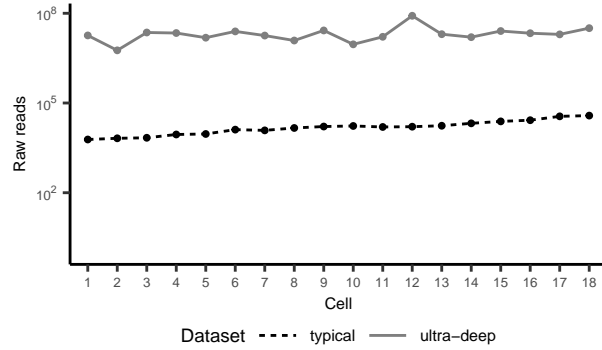


Figure 2: Raw read counts per cell before (*typical*) and after (*ultra-deep*) amplification for the 18 selected cells in the cta-seq experiment.

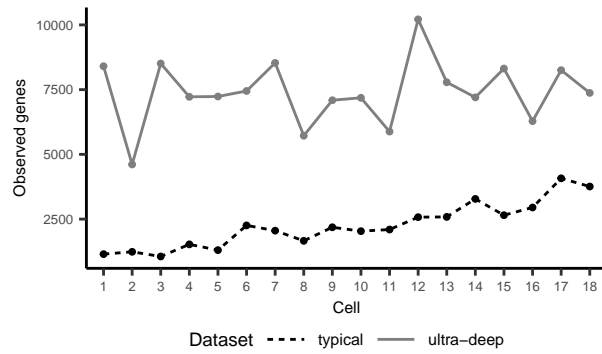


Figure 3: Number of observed genes before (*typical*) and after (*ultra-deep*) amplification for the 18 selected cells in the cta-seq experiment.

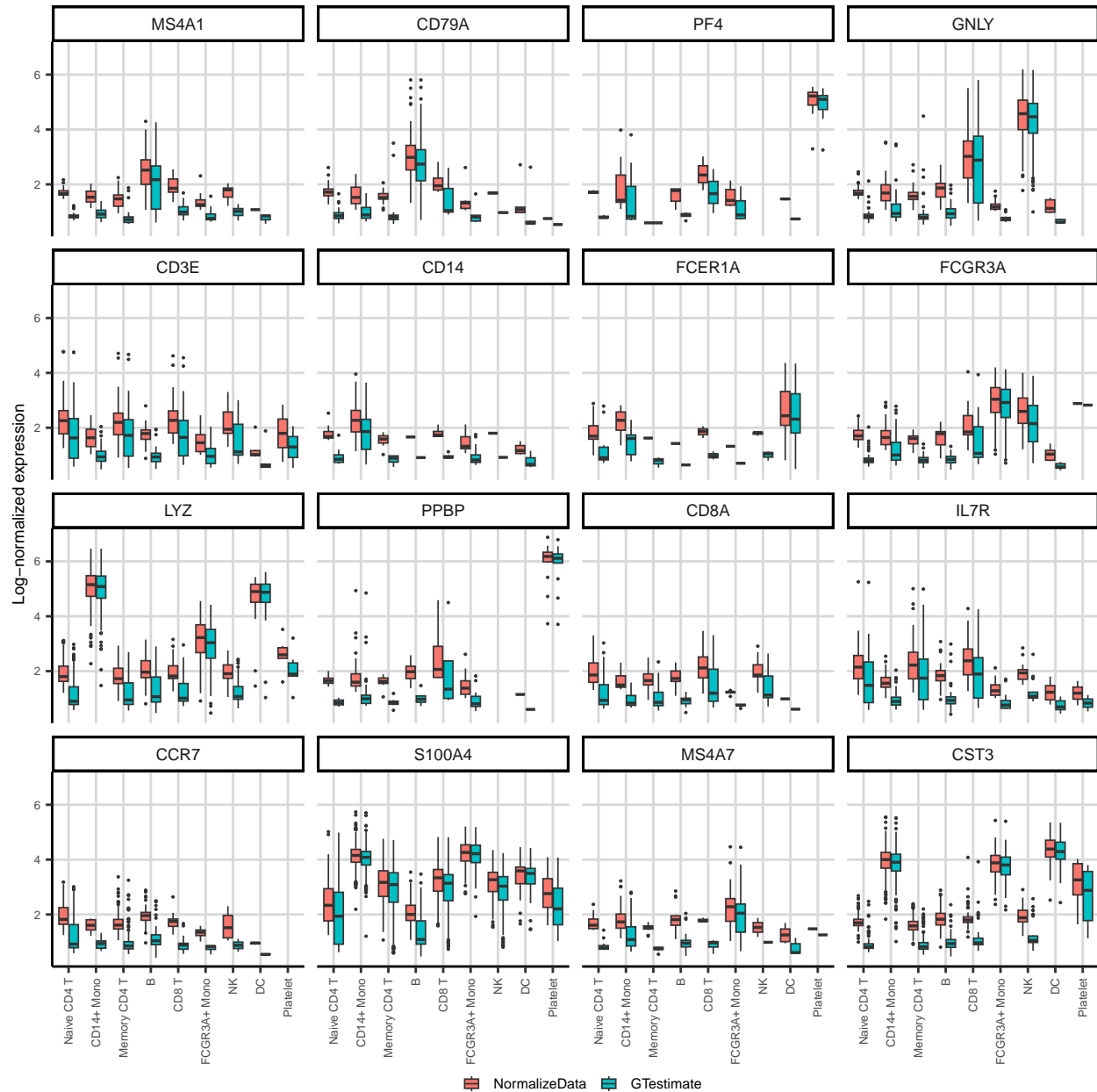


Figure 4: Log-normalized expression of all cell-type markers described in Seurat's pbmc3k tutorial (zeroes not shown).

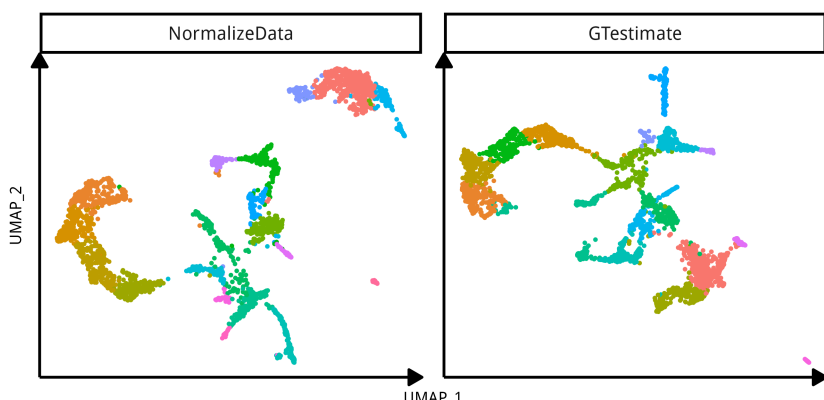


Figure 5: UMAPs visualizing the clustering of Spatial Transcriptomics spots, based on *NormalizeData* (left) and *GTestimate* (right) for the mouse brain Spatial Transcriptomics data-set.

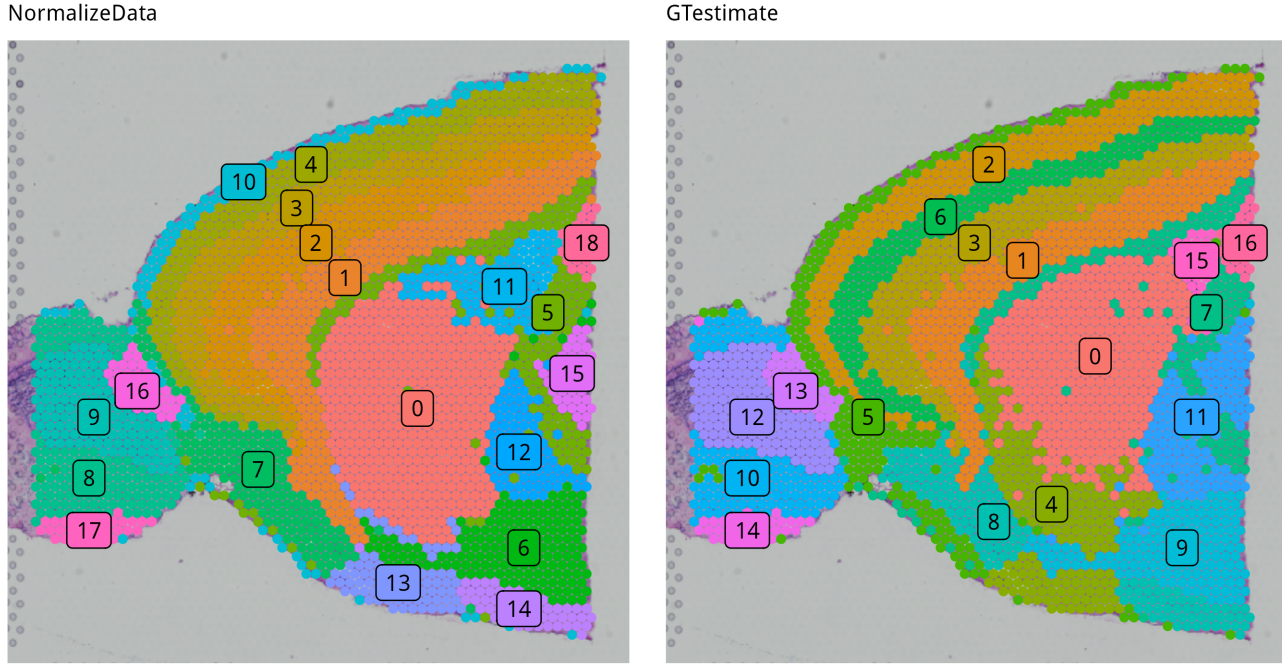


Figure 6: Visualization of the different clusters based on *NormalizeData* (left) and *GTestimate* (right) for the mouse brain Spatial Transcriptomics data-set.

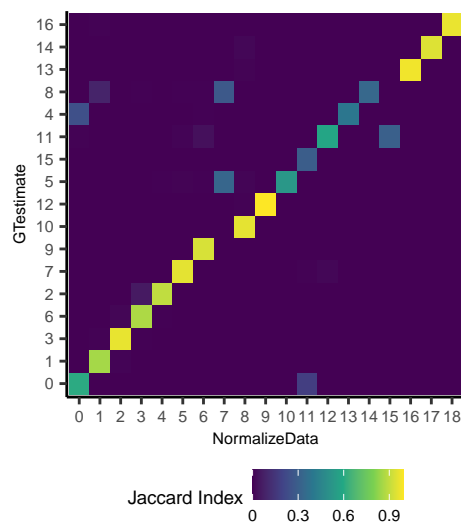


Figure 7: Similarity of the clusters based on *NormalizeData* and *GTestimate* as represented by the Jaccard Index. Clusters on the y-axis have been rearrange to maximize diagonal entries using the Hungarian Algorithm.

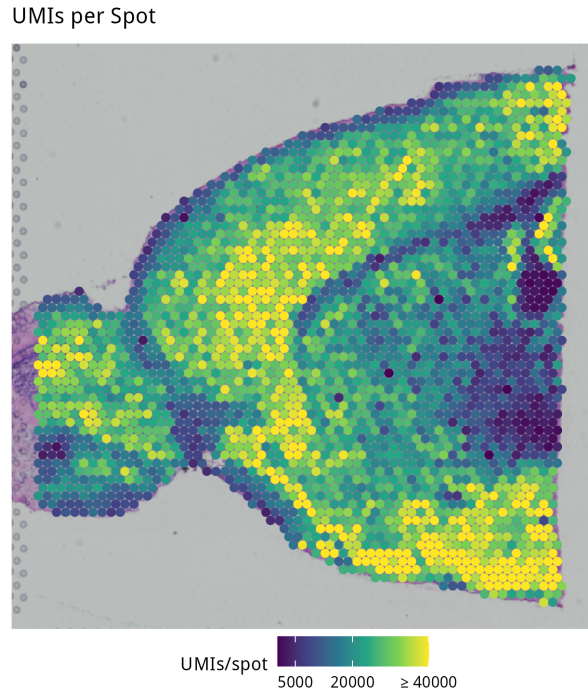


Figure 8:  $UMIs/spot$  in the Spatial Transcriptomics mouse brain data-set.

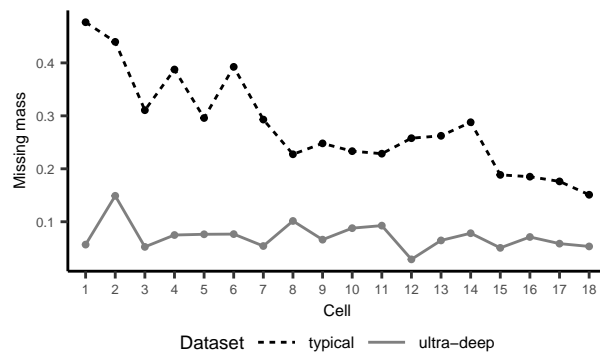


Figure 9: Missing mass before (*typical*) and after (*ultra-deep*) amplification for the 18 selected cells in the cta-seq experiment (see Suppl. Section 1.1).

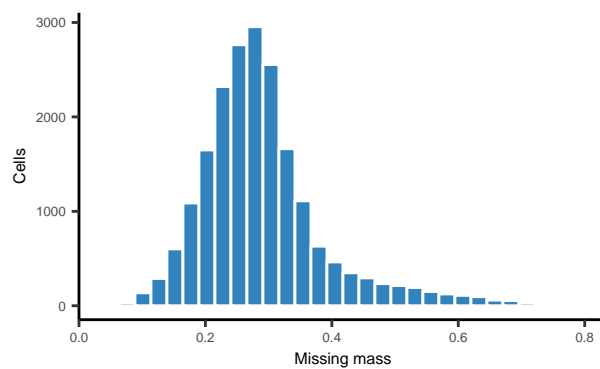


Figure 10: Histogram showing *GTestimate*'s missing mass estimates per cell for the 17,653 cells in the cta-seq sample before amplification (*typical*).